Single Stack Active Region Nonlinear Quantum Cascade Lasers for Improved THz Emission

(Invited Paper)

Frederic Demmerle, *Student Member, IEEE*
Jochen Bissinger
Wolfhard Oberhausen
Dominik Burghart
Jonas Krakofsky
Hannes Schmeiduch
Gerhard Boehm
M.-C. Amann, *Fellow, IEEE*

Single Stack Active Region Nonlinear Quantum Cascade Lasers for Improved THz Emission

(Invited Paper)

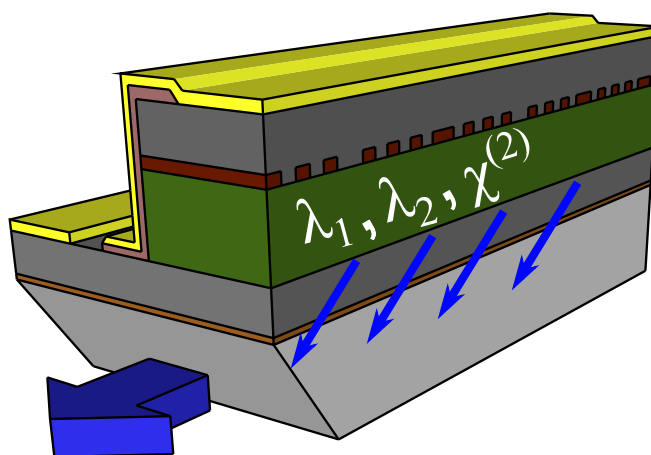**Frederic Demmerle, *Student Member, IEEE*, Jochen Bissinger, Wolfhard Oberhausen, Dominik Burghart, Jonas Krakofsky, Hannes Schmeiduch, Gerhard Boehm, and M.-C. Amann, *Fellow, IEEE***

Walter Schottky Institut, Technische Universität München, Garching D-85748, Germany

Abstract: We present a single stack active region design for terahertz emission by difference frequency generation in quantum cascade lasers. The active region contains a single design, which is based on multiple optical transitions within one period. This results in both a giant nonlinearity and an ultra-broad optical gain. The provided optical gain spectrum is broad enough to support two distinct mid-infrared modes with a significant spectral separation. For dual-emission, the waveguide contains a buried, index-coupled distributed feedback grating. This grating is based on a sampled approach to provide selective feedback for two mid-infrared modes at $\lambda_1 = 8.39\,\mu$m and $\lambda_2 = 9.38\,\mu$m. Simultaneously, the manifold of possible transitions within the active region is designed to provide a peak nonlinear susceptibility of $|\chi^{(2)}| = 29$ nmV^{-1} at the conversion to 3.8 THz. The device emits up to 210-μW THz power at room temperature with a nonlinear conversion efficiency of $\eta = 2.05$ mWW^{-2}.

Index Terms: Quantum cascade lasers, terahertz sources, nonlinear optical effects in semiconductors.

1. Introduction

Theterahertz (THz) range offers many interesting applications in sensing and scanning [1], yet the few available sources lack the convenience of a compact, efficient and easy to operate device. An emerging technology for semiconductor based THz sources is THz by difference-frequency generation (DFG) in quantum cascade lasers (QCLs) [2]. The crucial part is the utilization of an active region for the mid-infrared (MIR), which operates well at room temperature [3] contrary to its direct THz counterpart [4]. QCLs emitting in the MIR are well established and easily generate several watts of output power, which perfectly qualifies them to serve as optical pumps for a nonlinear process such as DFG. The nonlinear medium in DFG-QCLs is the active region itself, as the same electron states used for the optical transitions can be designed to possess giant nonlinear properties [5], [6]. This allows for monolithic integration of the nonlinear medium, which leads to a compact and robust device design with no external components. Additionally, the intracavity nonlinearity results
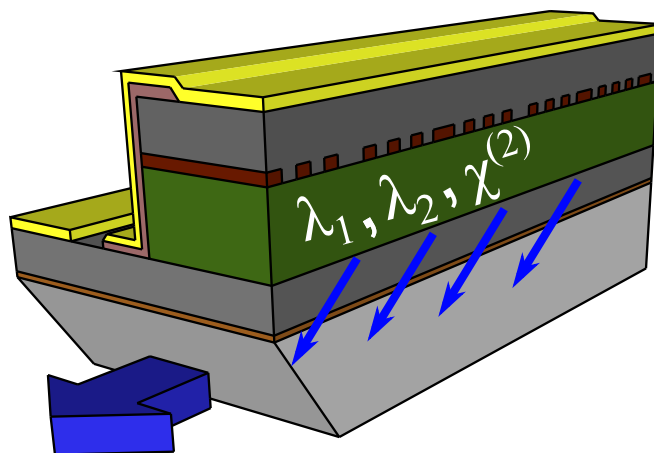
Fig. 1. Schematic drawing of the device with a single stack active region (green). Generated THz radiation (blue) leaks from the active region into the low-loss substrate. The front facet is polished to 30° to compensate for the Cherenkov angle of the substrate guided THz.

in a large spatial overlap with the high field intensities of the MIR pump wavelengths within the cavity, yielding a higher conversion efficiency than external cavity nonlinearities.

For the THz extraction, state of the art devices rely on Cherenkov phase matching (CPM) [7]. This allows the THz mode to leak from the highly absorbent active region and propagate in the low-loss semi-insulating substrate, which leads to a significantly higher output power due to enhanced extraction of the generated THz radiation as depicted in Fig. 1. As two MIR wavelengths are required for the nonlinear conversion process and their energy spacing corresponds to the generated THz frequency, the necessary gain requires a much broader spectral width in the MIR than a conventional single wavelength QCL provides. A common approach to address this problem is implementing two separate active regions stacked on top of each other. This is a unique possibility of the QCL, as due to its unipolar nature both active regions are supplied with the same current by the cascading electron scheme. In such stacked active region concept, each active region is optimized for one single wavelength while additionally providing a giant nonlinear susceptibility $\chi^{(2)}$. As the index-guided modes overlap multiple stacks of the active region, the resulting sum optical gain is broad enough to support dual-emission. However, this approach is prone to lasing at unwanted wavelengths as the sum gain shifts the gain peaks away from the desired resonances and induces gain peaks at undesired wavelengths. Lasing at these unwanted wavelengths have to be suppressed with selective feedback mechanisms at the cost of energy. Furthermore, the resulting nonlinearity is the sum of two different sets of intersubband transitions, which makes it impossible for the MIR pumps to be resonant with both integrated nonlinearities at the same time. Single stack active region designs significantly simplify the active region by fitting all requirements into a single design for the active region, but so far have demonstrated moderate nonlinear conversion efficiencies [8]. We present a single stack active region, which provides the advantage of a compact design and an improved nonlinear conversion efficiency.

2. Device Design

The demonstrated active region consists of a single design, which provides both optical gain and a giant nonlinearity. Compared to active region designs which are used in the stacked active region approaches, this design provides an ultra-broadband MIR gain to support two wavelengths simultaneously. Considering the intersubband structure of the design, this is achieved by creating a two-fold optical transition with the same upper laser state (1) utilizing two separate lower laser states (2) and (3) with equally strong transitions, as depicted in Fig. 2. For the sake of comparison, we use stack A of the stacked active region approach from reference [9] and modify with the presented
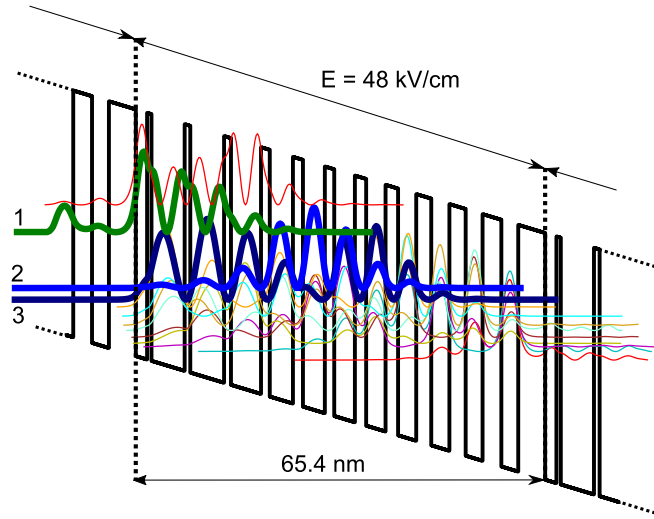
Fig. 2. Subsequent periods of the nonlinear active region design using AlInAs/GaInAs lattice-matched on InP. The thicknesses in nm are **4.3**/1.8/**0.7**/5.3/**0.9**/5.4/**1.1**/4.8/**1.4**/3.7/**1.6**/3.5/**1.5**/3.3/**1.8**/3.1/**2**/2.9/**2.4**/2.9/ **2.6**/2.7/**3**/2.7 where underlined thicknesses represent doped layers (2 x 10^{17} cm^{-3}). The three bold wave functions indicate the main optical transitions, which are used in this design, with one upper state (1) and two lower states (2) and (3).

design strategy. This allows a direct comparison of both design strategies in terms of theoretical properties and experimental values. The isolated upper laser state is created by a thin well adjacent to the injection barrier as in the well-known bound-to-continuum design [10]. Thus, the complex equation for intersubband gain of multi quantum well structures [11] can be well approximated by taking into account only the upper laser state (1) with multiple lower laser states

$$g(\omega_i) = \frac{\omega_i}{c \cdot n_{\text{eff}}(\omega_i)} \frac{\Delta N}{\hbar \epsilon_0} \Im \left(\sum_n \frac{|e \cdot z_{1n}|^2}{(\omega_i - \omega_{1n} - i \cdot \Gamma_{1n})} \right) \tag{1}$$

where ez_{1n}, ω_{1n} and Γ_{1n} are the dipole matrix element, frequency and broadening of the transition between the upper laser state (1) and laser state n. The broadening of the transitions is assumed as $\Gamma_{1n} = 12.5$ meV. In the presented active region, the resulting intersubband gain is designed to provide equal optical gain for the two optical modes in the spectral region of 8.5 μm and 9.5 μm.

Calculations of the intersubband gain are shown in Fig. 3. At the design field strength of 48 kVcm^{-1}, the gain profile results in a symmetric and relative flat MIR gain profile. This is crucial, as any surplus of gain in unwanted regions needs to be suppressed at the cost of pump energy. Due to finite electron transport in the active region, the active region bias further increases past reaching the design point. Therefore, the design is investigated for bias strengths above and below the intended operation point. At field strengths below the optimum of 48 kVcm^{-1}, the optical transition for the shorter wavelength is stronger, resulting in a higher optical gain for the shorter wavelength. This characteristic inverts with a higher applied bias. While an equal gain is achieved at the design field strength, the optical gain shifts towards longer wavelengths at higher field biases, favoring the longer mode.

Simultaneously, the manifold of possible intersubband transitions within one period results in a second order nonlinear susceptibility $\chi^{(2)}$ [12] which can be as large as 39.7 nmV^{-1} [13]. The largest contribution to this nonlinear susceptibility is by the strongest transitions between the discrete electron states, which are the optical transitions itself. Thus, the THz frequency with the highest conversion efficiency corresponds to the anticrossing of the two lower laser states (2) and (3) of Fig. 2. Assuming most of the electron population in the upper laser state (1), the second-order
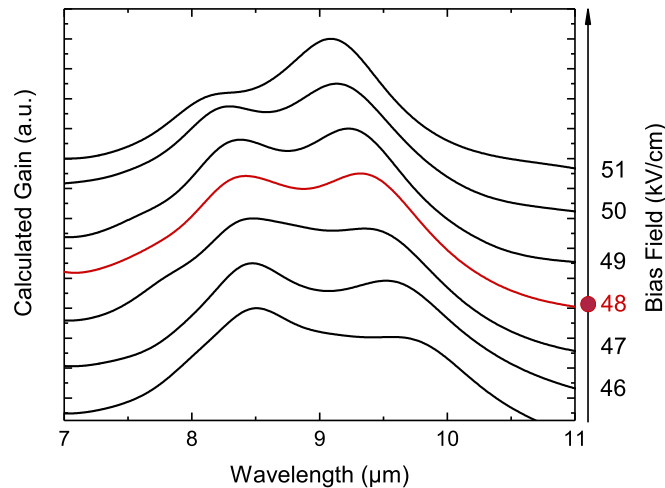
Fig. 3. Calculated spectral gain at different applied bias fields. The active region shows a symmetric gain profile at the designed bias field of 48 kV/cm (red). Below the design field strength, the calculated gain profile shows an asymmetric distribution with a higher optical gain around 8.5 μm. Towards higher bias fields, this characteristic is inverted with a significant favoring of optical gain in the spectral region of 9.5 μm.

nonlinear susceptibility can be simplified to

$$\chi_{xxx}^{(2)}(\omega_3 = \omega_1 - \omega_2) \approx \Delta N \frac{e^3}{\hbar^2 \epsilon_0} \frac{z_{12} z_{31} z_{23}}{(\omega_3 - \omega_{23} + i\Gamma_{23})} \left(\frac{1}{\omega_1 - \omega_{13} + i\Gamma_{31}} + \frac{1}{-\omega_2 + \omega_{12} + i\Gamma_{21}} \right) \quad (2)$$

where ΔN is the population inversion density, ez_{ij}, ω_{ij} and Γ_{ij} are the dipole matrix element, the frequency and broadening of the transition between states i and j. By utilizing only one active region design, both pumps can achieve perfect resonance to this monolithic integrated nonlinearity. The peak nonlinear susceptibility is calculated to reach $\chi^{(2)} = 29$ nmV^{-1} for the resonant case, assuming $\Gamma_{21} = \Gamma_{31} = 12.5$ meV and $\Gamma_{23} = 4$ meV. This value is higher by a factor of 1.25 compared to other design strategies involving multiple transitions within one period [8]. For an efficient MIR to THz conversion, a high spectral purity of the MIR pump wavelengths is essential. Furthermore, the very broad gain spectrum of the optical active medium requires selective feedback in order to achieve lasing at distinct wavelengths. This is achieved by a distributed feedback (DFB) grating. The grating is realized as an index-coupled grating, where the real part of the refractive index is varied along the propagation direction through a patterned InGaAs layer with a higher refractive index than the surrounding InP. The structured grating is buried beneath the upper wavecladding for optimum coupling. As two MIR wavelengths are required, a sampled grating is used to achieve dual response at the desired wavelengths [14]. Furthermore, an additional phase shift at the center of the grating is introduced, which leads to a single central mode at a defined wavelength [15].

3. Fabrication

The first epitaxial step includes the lower wave cladding (3 μm n-InP, doped 1.5×10^{16} cm^{-3}), active region and the InGaAs DFB layer grown by molecular beam epitaxy (MBE) on semi-insulating InP. For the active region, the design for one period is grown 66 times in order to achieve a total thickness of 4.4 μm. The DFB layer consists of 400 nm n-InGaAs doped with 1.5×10^{16} cm^{-3} and the grating is structured by electron beam lithography and subsequently etched by reactive ion-etching (RIE). Additional overgrowth was performed by metalorganic chemical vapor deposition (MOCVD) to complete the structure with an upper 3 μm InP wavecladding doped with 1.5×10^{16} cm^{-3} and a 50 nm highly doped InGaAs contact layer. Afterwards, the laser is processed as a conventional
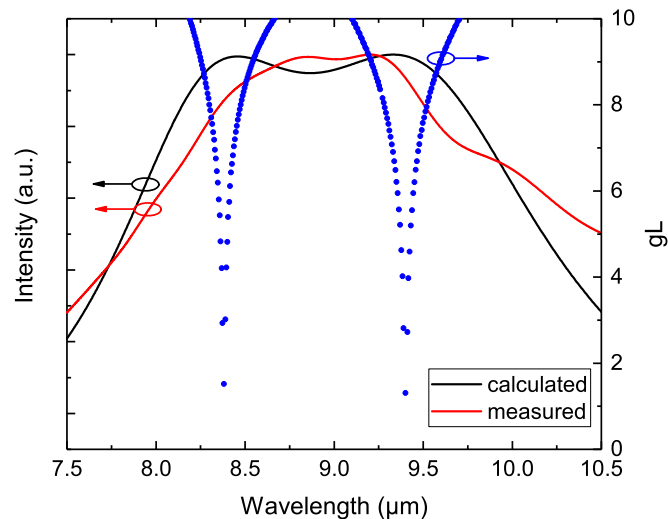
Fig. 4. Calculated gain at the designed bias field and the corresponding electroluminescence measurement of the sample. In accordance to the electroluminescence, the grating is designed to provide selective feedback for two central modes at 8.38 μm and 9.4 μm with equal optical gain gL (blue).

edge emitter with a ridge width of 20 μm and cleaved into bars of 4.5 mm. Both facet ends are anti-reflection coated with a multilayer system of AlF and ZnS to achieve low reflectance for both MIR wavelengths simultaneously. In order to extract the generated THz radiation, the front facet is polished to 30° to compensate for the Cherenkov angle of $\theta_C \approx 20°$.

4. Results

First, electroluminescence (EL) samples are processed and measured to examine the gain profile of the structure. In Fig. 4 the calculated gain and the measured EL spectra are compared. Overall, the measurement shows good agreement with the calculation. The spectral broadness of the EL indicates a significant broader gain profile than the referenced stacked active region design [9]. The DFB gratings are designed in accordance with the EL curve with two central modes at 8.38 μm and 9.4 μm. The separation of both wavelengths is designed to result in a difference frequency at 3.8 THz. From the comparison of the EL spectrum with the calculated modes, it can be seen that at the design field strength both MIR modes are supported equally by the provided optical gain. The spectral region between the two modes shows no additional gain peaks. Subsequently, THz DFG-QCLs in the CPM configuration were fabricated with a length of 4.5 mm and a ridge width of 20 μm.

Spectral measurements in the MIR yield two distinct peaks as depicted in Fig. 5. The wavelengths at 8.39 μm and 9.38 μm are well within the range of the refractive index calculation and correspond to the modes selected by the grating. In the range of the longer mode, an additional lasing peak is found at a shorter wavelength of 9.31 μm with an attenuation of -16 dB. Considering the ridge width of 20 μm, it can be shown that this wavelength is the 1st order lateral mode to the ground mode at 9.38 μm. Although not desired for the MIR pumps, it is irrelevant to the THz spectrum. The 1st order lateral mode will not contribute to a nonlinear conversion process due to the lack of spatial overlap with a second wavelength which is required for DFG. Spectral THz measurements show single mode emission at 3.77 THz and is plotted in Fig. 6. The THz frequency corresponds to the spectral separation of the MIR pumps. No additional THz frequencies are found in the spectrum, which further indicate the lack of spatial overlap of the 1st order lateral mode with a second mode.

Power measurements of the device are shown in Fig. 7. All power measurements are recorded at room temperature, while the device was working in pulsed mode with a pulse width of 50 ns and a repetition rate of 25 kHz. The setup consists of two off-axis parabolic mirrors and appropriate
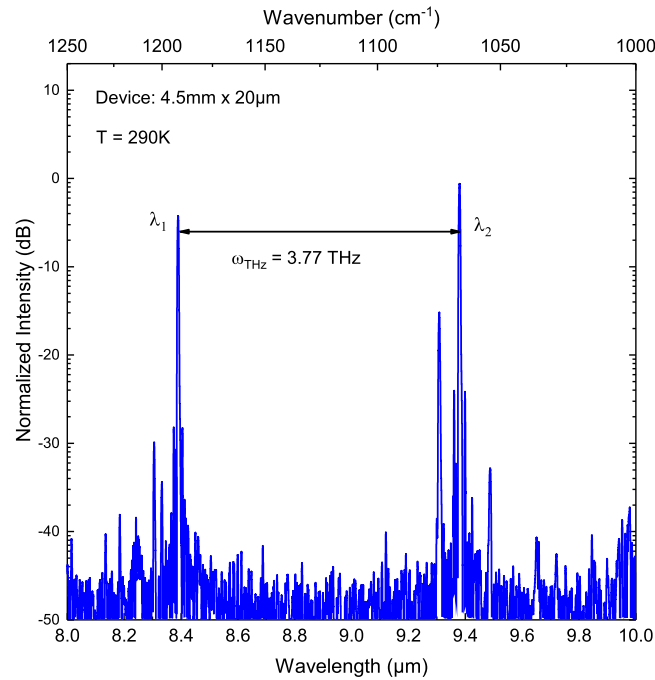
Fig. 5. Spectral measurements of the MIR output of the device show emission of two distinct wavelengths at 8.39 μm and 9.38 μm in accordance with the dual-response of the sampled DFB grating.
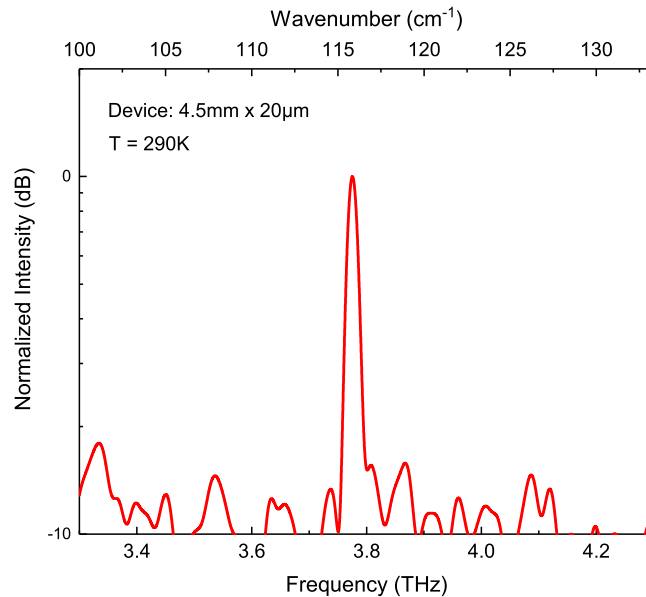

Fig. 6. Spectral measurements of the generated THz radiation show single mode emission at 3.77 THz at room temperature. The THz frequency is in perfect accordance to the spectral separation of the MIR pumps.

detectors for the MIR and THz. All measurements are corrected for filter transmission, as this characteristic is well known. Furthermore, a correction for collection efficiency of 70% of the setup was applied. This is an approximation, as the exact collection efficiency is difficult to determine accurately and is likely to be lower in the case of THz detection, due to the divergent far field.
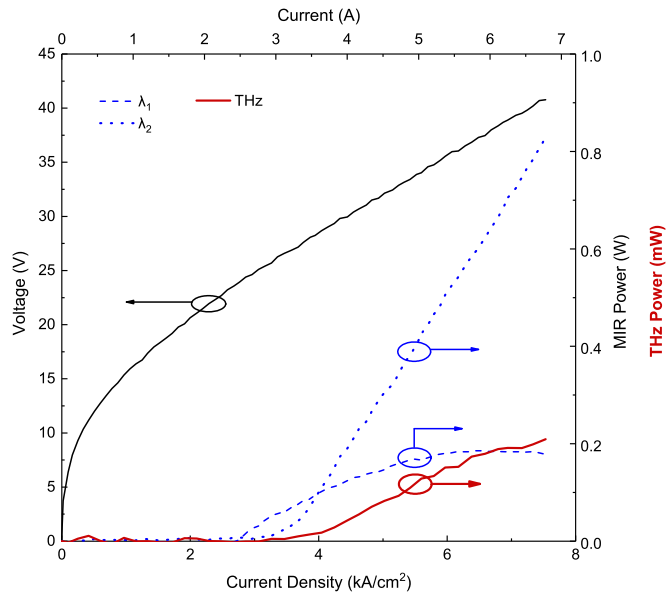
Fig. 7. Power measurements of the MIR emission yield a combined optical peak power of 1 W. Optical filters were used to separate the optical power of both pumps. An unequal distribution of optical power is found, as the short wavelength reaches rollover point at 1/4 of the maximum power of the long wavelength. The optical power of the generated THz is measured with the onset of the second wavelength and peaks at 210 μW.
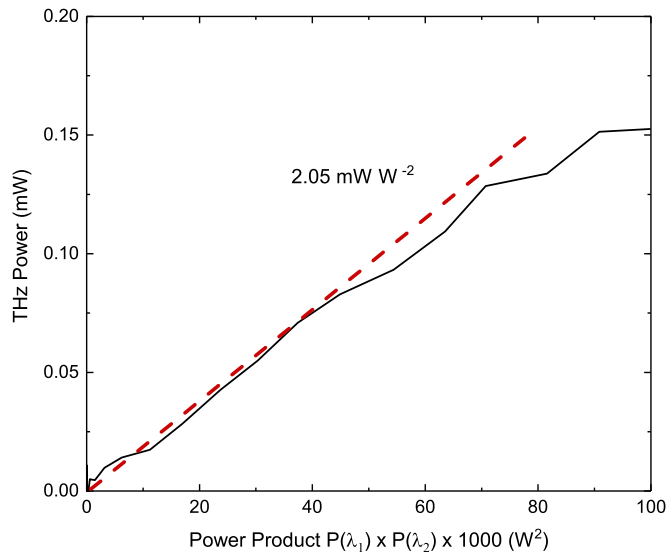

Fig. 8. Plotting the emitted THz power over the power product $\boldsymbol{P}(\lambda_1) \times \boldsymbol{P}(\lambda_2)$ yields a nonlinear conversion efficiency of 2.05 mWW^{-2}. This high nonlinear conversion efficiency is attributed to the high nonlinear susceptibility of the active region.

For the MIR measurements, an optical high pass filter was used to separate both pump wavelengths. While dual-emission is achieved over almost the entire operation range, the optical power is distributed unequally with a significant favoring of the longer wavelength towards higher currents. Considering threshold currents, it is found that the shorter wavelength has a smaller threshold, but a lower external quantum efficiency and a lower total optical power. This behavior is in accordance to the gain analysis of Fig. 3. At lower field biases, the short wavelength is provided with more gain leading to an earlier threshold of this wavelength. Operating past the optimum field bias of

48 kVm^{-1}, the gain shifts towards the longer wavelength region leading to a higher optical output power of the corresponding wavelength. The power measurement of the generated THz radiation was recorded with a calibrated Golay cell. A total power of 210 μW is recorded. As can be seen from Fig. 8, this translates to a nonlinear conversion efficiency of 2.05 mWW^{-2}. Compared to DAU-type devices, this is an improvement of the nonlinear conversion from 0.8 mWW^{-2}. Besides the increased nonlinear susceptibility $\chi^{(2)}$, the use of a larger volume of nonlinear medium and a shorter wavelength pairing leads to an improved modal overlap compared to the DAU device from [8]. Both design improvements eventually contribute to a larger nonlinear conversion efficiency.

5. Conclusion

In conclusion, we have demonstrated that it is possible to use a single active region design to achieve both optical gain and a giant nonlinearity. With multiple optical transitions within one period, the resulting optical gain is broad enough in order to support two distinct wavelengths, which can be selected with a sampled DFB grating with dual-response. As only one active region design is used, perfect resonance of both MIR pumps with the monolithic integrated nonlinearity can be achieved, which eventually translates into a higher nonlinear conversion efficiency. With this design strategy, we have achieved an increased nonlinear susceptibility of $|\chi^{(2)}| = 29$ nmV^{-1} with a corresponding increased conversion efficiency of 2.05 mWW^{-2}. At room temperature, the device emits up to 210 μW while operating in pulsed mode. Compared to the reference, this is a significant increase in both absolute THz power and nonlinear conversion efficiency. Current state of the art THz DFG QCLs achieve mW level THz output power mainly through sheer optical MIR power but with nonlinear conversion efficiencies below 1 mWW^{-2} [13], [16]. We have demonstrated a design strategy leading to a significant higher nonlinear conversion efficiency at a relatively small cost of optical power in the MIR, potentially increasing THz power beyond these state of the art devices. Further optimization includes the design field strength at higher biases. Although this will further increase the disparity of threshold currents of the two MIR pumps, the absolute THz power will eventually be higher based on a more uniform distribution of optical power among the two MIR optical pump modes.

Acknowledgment

References

[1] M. Tonouchi, "Cutting-edge terahertz technology," *Nature Photon.*, vol. 1, pp. 97–105, 2007.
[2] M. A. Belkin *et al.*, "Terahertz quantum-cascade-laser source based on intracavity difference-frequency generation," *Nature Photon.*, vol. 1, no. 5, pp. 288–292, 2007.
[3] M. A. Belkin *et al.*, "Room temperature terahertz quantum cascade laser source based on intracavity difference-frequency generation," *Appl. Phys. Lett.*, vol. 92, no. 20, 2008, Art. no. 201101.
[4] S. Fathololoumi *et al.*, "Terahertz quantum cascade lasers operating up to 200 K with optimized oscillator strength and improved injection tunneling," *Opt. Exp.*, vol. 20, no. 4, 2012, Art. no. 3866.
[5] E. Rosencher and P. Bois, "Model system for optical nonlinearities: Asymmetric quantum wells," *Phys. Rev. B*, vol. 44, no. 20, pp. 11315–11327, 1991.
[6] C. Sirtori, F. Capasso, J. Faist, L. N. Pfeiffer, and K. W. West, "Far-infrared generation by doubly resonant difference frequency mixing in a coupled quantum well two-dimensional electron gas system," *Appl. Phys. Lett.*, vol. 65, no. 4, pp. 445–447, 1994.
[7] K. Vijayraghavan *et al.*, "Terahertz sources based on Čerenkov difference-frequency generation in quantum cascade lasers," *Appl. Phys. Lett.*, vol. 100, 2012, Art. no. 251104.
[8] K. Fujita *et al.*, "Terahertz generation in mid-infrared quantum cascade lasers with a dual-upper-state active region," *Appl. Phys. Lett.*, vol. 106, no. 25, pp. 16–20, 2015.
[9] K. Vijayraghavan *et al.*, "Broadly tunable terahertz generation in mid-infrared quantum cascade lasers," *Nature Commun.*, vol. 4, 2013, Art. no. 2021.
[10] J. Faist, M. Beck, T. Aellen, and E. Gini, "Quantum-cascade lasers based on a bound-to-continuum transition," *Appl. Phys. Lett.*, vol. 78, no. 2, pp. 147–149, 2001.
[11] C. Jirauschek and T. Kubis, "Modeling techniques for quantum cascade lasers," *Appl. Phys. Rev.*, vol. 1, no. 1, 2014, Art. no. 011307.
[12] R. W. Boyd, *Nonlinear Optics*. Orlando, FL, USA: Academic, 2008.

[13] Q. Lu and M. Razeghi, "Recent advances in room temperature, high-power terahertz quantum cascade laser sources based on difference-frequency generation," *Photonics*, vol. 3, no. 3, Jul. 2016, Art. no. 42.

[14] Q. Y. Lu, N. Bandyopadhyay, S. Slivken, Y. Bai, and M. Razeghi, "Widely tuned room temperature terahertz quantum cascade laser sources," *Appl. Phys. Lett.*, vol. 101, 2012, Art. no. 251121.

[15] J. Buus, D. J. Blumenthal, and M.-C. Amann, *Tunable Laser Diodes and Related Optical Sources*, vol. 1. New York, NY, USA: Wiley, 2005.

[16] Q. Lu, D. Wu, S. Sengupta, S. Slivken, and M. Razeghi, "Room temperature continuous wave, monolithic tunable THz sources based on strain-balanced mid-infrared quantum cascade lasers," *Sci. Rep.*, vol. 6, pp. 1–16, 2016.